

The Baryonic Tully-Fisher Relation of HI-bearing Low Surface Brightness Galaxies Implies Their Formation Mechanism

Zichen Hua^{1,2}, Yu Rong^{1,2*}, Huijie Hu^{3,4}

¹Department of Astronomy, University of Science and Technology of China, Hefei 230026, China

²School of Astronomy and Space Sciences, University of Science and Technology of China, Hefei 230026, China

³University of Chinese Academy of Sciences, Beijing 100049, China

⁴National Astronomical Observatories, Chinese Academy of Sciences, Beijing 100012, China

Accepted November 28, 2024. Received March 25, 2024.

ABSTRACT

We investigate the baryonic Tully-Fisher relation in low surface brightness galaxies selected from the Arecibo Legacy Fast ALFA survey. We find that the HI-bearing low surface brightness galaxies still follow the baryonic Tully-Fisher relation of typical late-type galaxies, with a slope of approximately 4 in the baryonic mass versus rotational velocity diagram on the logarithmic scale, i.e., $M_b \propto v_{\text{rot}}^4$. Our findings suggest that the matter distributions in low surface brightness galaxies may resemble that of general late-type galaxies, and hint that low surface brightness galaxies may not originate from dark matter halos of low densities or stronger/weaker feedback processes, but may emerge from dark matter halos with high spin values.

Key words: galaxies: kinematics and dynamics – galaxies: formation – galaxies: evolution

1 INTRODUCTION

Low surface brightness galaxies (LSBGs) constitute a special population of galaxies with central surface brightness at least one magnitude fainter than that of the sky background (i.e., B -band surface brightness $\geq 22.5 \text{ mag} \cdot \text{arcsec}^{-2}$; Impey & Bothun 1997; Bothun et al. 1997). Many isolated LSBGs have been observed to exhibit higher HI fractions (e.g., Catinella et al. 2018; Schombert & McGaugh 2021; Du et al. 2015; He et al. 2020). However, some studies (e.g., Martin et al. 2019; Galaz et al. 2002) alternatively found that some LSBGs exhibit the same or even smaller gas fractions compared to high surface brightness galaxies (HSBGs). LSBGs usually have low star formation rates (Wyder et al. 2009; Rong et al. 2020b), low metallicities (Kuzio de Naray et al. 2004; Schombert & McGaugh 2021), and tend to appear in low-density environment (Pérez-Montaño & Cervantes Sodi 2019; Mo et al. 1994; Galaz et al. 2011).

The formation mechanism of LSBGs, which plays a crucial role in refining our empirical galaxy formation models, have gathered much attention ever since their initial detection. Early studies often regarded LSBGs as galaxies formed in low-density dark matter halos (Dekel & Silk 1986; McGaugh 1992; Mo et al. 1994). However, recent studies have presented more alternative scenarios. One classical formation scenario is that LSBGs are galaxies hosted in dark matter halos with higher halo spin. In cosmological simulations, the halos of LSBGs are found to have higher spin parameters compared with HSBGs, regardless of whether they are relatively massive (Mo et al. 1998; Kim & Lee 2013; Kulier et al. 2020; Pérez-Montaño et al. 2022), or belong to ultra-diffuse galaxies (UDGs, Rong et al. 2017; Amorisco & Loeb 2016; Rong et al. 2024) – a specific subset of

LSBGs of smaller masses (e.g., van Dokkum et al. 2015a, 2018; Mancera Piña et al. 2018, 2019). Additionally, some studies suggest that low-mass LSBGs may represent failed L^* galaxies (van Dokkum et al. 2015a,b), or originate from early co-planar mergers (Wright et al. 2021) or stellar feedback processes (Chan et al. 2018; Di Cintio et al. 2019), or birth during tidal interactions (Rong et al. 2020a; Carleton et al. 2019), or form through multiple pathways (Papastergis et al. 2017). High-mass LSBGs, alternatively, may form through mergers (Saburova et al. 2018; Di Cintio et al. 2019; Zhu et al. 2023), two-stage process with external gas accretions (Saburova et al. 2021), or dynamical evolution driven by bars (Noguchi 2001).

Nevertheless, despite extensive efforts, our present comprehension of the formation and evolution of LSBGs is still limited. One of the key reasons is that studies on the mass distributions and baryonic fractions in LSBGs have not achieved a consensus, and a comprehensive scenario has not been established to constrain the current formation and evolution models of LSBGs. Many studies have shown that the dynamics of LSBGs may be dominated by dark matter (e.g., de Blok & McGaugh 1997; Mowla et al. 2017; Swaters et al. 2003; Read et al. 2017; Mancera Piña et al. 2022), yet UDGs may exhibit a deficiency in dark matter content (e.g., van Dokkum et al. 2018; Mancera Piña et al. 2019). As for the stellar-to-halo mass relation ($M_* - M_h$), while Prole et al. (2019) propose that LSBGs form a continuous extension of typical dwarfs in the $M_* - M_h$ diagram, other studies reveal significant deviations for UDGs from the typical $M_* - M_h$ relation (e.g., van Dokkum et al. 2018). Additionally, some giant LSBGs appear to be dominated by baryons at their central regions, akin to the HSBG counterparts (e.g., Lelli et al. 2010; Saburova et al. 2021, 2019); the stellar-to-halo mass relation of the giant LSBGs and HSBGs also exhibits a similarity. All of these confusing signs of diversity in matter distribution among LSBGs could offer valuable insights

* Corresponding author; E-mail: rongyua@ustc.edu.cn

into their varied formation and evolution pathways. Consequently, a comprehensive understanding of the matter distributions in LSBGs is essential for refining our current models of galaxy formation and evolution.

The baryonic Tully-Fisher relation (BTFR) is a correlation between the rotational velocity, v_{rot} , and the baryonic mass, M_b , of galaxies. Over the past two decades, many studies have shown that late-type galaxies and dwarf galaxies consistently adhere to a power-law form of BTFR, despite their wide ranges of baryonic mass, luminosity, and size. BTFR could be written as, $M_b \propto v_{\text{rot}}^\beta$, where the logarithmic slope, β , typically falls within a range from 3 to 4 (e.g., [McGaugh et al. 2000](#); [Verheijen 2001](#); [Begum et al. 2008](#); [Papastergis et al. 2016](#); [Lelli et al. 2016a](#); [Sales et al. 2017](#); [Ponomareva et al. 2018](#); [Goddy et al. 2023](#)). Notably, some studies have also discovered that early-type galaxies may also follow the BTFR of late-type galaxies ([den Heijer et al. 2015](#); [Serra et al. 2012](#)).

In the context of Λ CDM paradigm, the presence of BTFR is considered as a correlation between the virial velocity of the dark matter halo and the baryonic mass enclosed within that halo ([McGaugh 2012](#); [Mo et al. 1998](#)). Thus, it can serve as a valuable tool to probe the distribution of baryonic matter and dark matter within galaxies. Furthermore, simulations have highlighted the significance of feedback processes in shaping the observed BTFR (e.g., [Governato et al. 2010](#); [Piontek & Steinmetz 2011](#); [Dutton 2012](#)), suggesting that investigating the BTFR can serve as a valuable means to constrain the feedback mechanisms at work within galaxies. Additionally, BTFR is highly related to other dynamical relationships such as the radial acceleration relation (e.g., [McGaugh et al. 2016](#); [Lelli et al. 2017](#)). Exploring the BTFR could also provide insights into new gravitational theories, as a BTFR with $\beta = 4$ is well predicted by the Modified Newtonian Dynamics (MOND, [Milgrom 1983](#)). Given its multifaceted implications, the BTFR remains one of the most extensively studied dynamical relations in astrophysics.

As anticipated, recent studies examining the BTFR of LSBGs also show some potential signs of tension. Previous studies have found that the BTFR does not depend on galactic surface brightness or other galactic properties (e.g., [Lelli et al. 2016a](#); [Ponomareva et al. 2018](#); see also [Zwaan et al. 1995](#)). However, some recent investigations (e.g., [Mancera Piña et al. 2019](#); [Guo et al. 2020](#); [Hu et al. 2023](#); [Karunakaran et al. 2020](#); [Rong et al. 2024](#)) reveal that, the particular subsample of LSBGs with large disk sizes, i.e., UDGs, may significantly deviate from the BTFR of typical late-type galaxies, indicative of the possible dependence on size ([Mancera Piña et al. 2020](#)). Therefore, a thorough and meticulous examination of the BTFR for LSBGs becomes essential. Such an analysis may not only indicate whether the matter distribution within LSBGs aligns with that of typical late-type and dwarf galaxies, but also provide valuable constraints on the formation mechanisms of LSBGs.

In this work, we will first introduce our sample selection in Section 2, and then describe our methods for calculating M_b and v_{rot} in Section 3. We will then present our results in Section 4, and finally discuss the potential selection biases and the possible formation mechanism of LSBGs in Section 5. The summary is in Section 6.

2 SAMPLE SELECTION

The Arecibo Legacy Fast ALFA survey (ALFALFA) is a wide-area blind HI survey aimed at searching for HI-bearing objects in the extragalactic neighbourhood. [Haynes et al. \(2011\)](#) matched the HI sources in the ALFALFA $\alpha.40$ catalogue with the optical catalogue of the Sloan Digital Sky Survey (SDSS) Data Release 7 (DR7), and

obtained the ALFALFA-SDSS $\alpha.40$ cross-matched catalogue. [Du et al. \(2015\)](#) and [He et al. \(2020\)](#) conducted precise photometry on these cross-matched galaxies in $\alpha.40$ catalog using their SDSS-DR7 g - and r -band images, obtaining the central surface brightness in the g - and r -bands, $\mu_0(g)$ and $\mu_0(r)$. The g - and r -band central surface brightness were further converted into B -band surface brightness based on ([Smith et al. 2002](#)),

$$\mu_0(B) = \mu_0(g) + 0.47 \times [\mu_0(g) - \mu_0(r)] + 0.17, \quad (1)$$

to select LSBGs. The authors finally selected a sample of LSBGs with the B -band apparent central surface brightness of $22.5 < \mu_0(B) < 27.64$ mag/arcsec², which is treated as the parent sample and used in this work to study the BTFR of LSBGs.

From the parent sample, we first remove LSBGs with g -band apparent axis ratios $b/a > 0.72$, approximately corresponding to the threshold of inclination angles of $i \lesssim 45^\circ$, because the face-on galaxies may introduce large uncertainties in the measurements of the rotation velocities (see equation (7)). We then exclude LSBGs with low HI spectral signal-to-noise ratios $\text{SNR} < 10$ (see [Haynes et al. 2018](#) for the definition of SNR). Furthermore, we exclude LSBGs with suspicious HI profiles that indicate potential interactions with other galaxies, serious asymmetric profiles, or profiles with data points affected by poor data quality, as illustrated in Fig. 1. The first two scenarios may suggest an in-equilibrium state of the galaxy, leading to inaccurate estimation of the rotation velocity.

Due to the bad spatial resolution of ALFALFA, if a galaxy has a close companion galaxy, its HI spectrum may be contaminated by the companion. To eliminate this possibility, we remove the galaxies with companions within the projected radii of $3.8'$ (i.e., approximately the beam size of Arecibo) and radial velocity differences of $\Delta v < 500$ km/s. The redshift of a LSBG is estimated from the central velocity of its HI spectrum¹, while the redshift of the neighbouring galaxies comes from the SpecObj and Photoz databases of SDSS. Finally, 204 LSBGs are left in our sample.

We also calculate the kurtosis coefficient, k_4 , of the HI spectrum ([Papastergis et al. 2016](#); [El-Badry et al. 2018](#)) for each galaxy, as

$$k_4 = M_4 / (\sigma^2)^2 - 3, \quad (2)$$

where M_4 and σ^2 are calculated as,

$$M_4 = \int_{v_{\text{min}}}^{v_{\text{max}}} (v - \bar{v})^4 F(v) dv / \int_{v_{\text{min}}}^{v_{\text{max}}} F(v) dv, \quad (3)$$

$$\sigma^2 = \int_{v_{\text{min}}}^{v_{\text{max}}} (v - \bar{v})^2 F(v) dv / \int_{v_{\text{min}}}^{v_{\text{max}}} F(v) dv. \quad (4)$$

Here, v and $F(v)$ represent the frequency and corresponding flux density, respectively. \bar{v} is defined as,

$$\bar{v} = \int_{v_{\text{min}}}^{v_{\text{max}}} v F(v) dv / \int_{v_{\text{min}}}^{v_{\text{max}}} F(v) dv. \quad (5)$$

where v_{min} and v_{max} correspond to the minimal and maximum frequencies between which W_{20} (see Section 3 for the definition of W_{20}) is measured, respectively. k_4 can distinguish the single-horned and double-horned spectra (see, e.g., Fig. 1 of [El-Badry et al. 2018](#)). The galaxies with single-horned HI lines may have kinematics strongly influenced by velocity dispersion ([El-Badry et al. 2018](#)) or beam smearing, or HI disks that are not extended enough to trace the flat part of the rotation curve ([Papastergis et al. 2016](#)). As a consequence, their HI-widths cannot represent the rotation velocities ([McGaugh](#)

¹ While the distances of our sample galaxies are obtained directly from [Haynes et al. 2018](#), please refer to their work for more details.

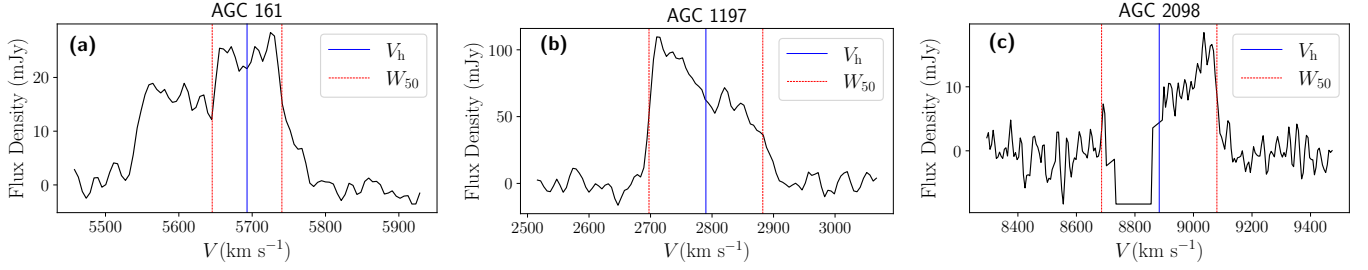


Figure 1. Examples of suspicious HI spectra from Haynes et al. (2018). V_h denotes the heliocentric velocity, and W_{50} denotes the 50% peak width of an HI spectrum, obtained by Haynes et al. (2018). Panel (a): a profile showing potential interactions with other galaxies. Panel (b): a seriously asymmetric profile. Panel (c): a profile containing bad points due to data quality.

2012; Verheijen 1997). Therefore, we perform a cut at the HI spectrum, $k_4 < -1$, in order to remove the galaxies with single-horned HI lines (see Fig. 3 of El-Badry et al. 2018 for the threshold).

The final sample contains 124 LSBGs with double-horned HI lines, ensuring the most reliable results. For comparison, 210 HSBGs with $\mu_0(B) < 22.5$ mag, and double-horned HI lines are selected from $\alpha.40$ as the counterparts. Fig. 2 presents various properties of our selected LSBGs and HSBGs, including g -band axis ratio b/a , average stellar-mass surface density within the g -band half-light radius $\langle \Sigma \rangle_{*,\text{eff}} = M_*/(2\pi R_{\text{eff}}^2)$ (see Section 3 for the stellar mass M_* estimation; R_{eff} is estimated following Rong et al. (2024)), $g-i$ color, gas fraction f_g ($f_g = M_g/M_b$; see Section 3 for the derivation of M_g), g -band stellar disk scale length $R_d = R_{\text{eff}}/1.678$, and baryonic mass M_b .

3 METHOD

The baryonic mass of a galaxy is mainly composed of the stellar mass and gas mass. The stellar mass M_* can be estimated with the galaxy luminosity in the $W1$ -band (denoted as L_{W1}) from the Wide-field Infrared Survey Explorer (Wright et al. 2010), using the method proposed by McGaugh & Schombert (2015), as

$$M_*/M_\odot = 0.45L_{W1}/L_\odot. \quad (6)$$

As for the gas mass, M_g , we estimate it by adding up the masses of HI and helium, where M_{HI} is the HI mass (see Haynes et al. 2018 for the method of estimating M_{HI}). The baryonic mass of a galaxy is then estimated as $M_b = M_* + M_g$. Note that M_b does not include the hot ionized gas and molecular gas, as their fractions are expected to be small compared to the HI fraction (McGaugh 2012; Zhong et al. 2023), and thus are negligible.

We use the 20% peak width of an HI spectrum (W_{20} ; Guo et al. 2020; Hu et al. 2023; Rong et al. 2024; see the *Method* section of Guo et al. (2020) for the method of estimation of W_{20}) to calculate the rotation velocity v_{rot} . Guo et al. (2020) have demonstrated that W_{20} can accurately trace galactic v_{rot} , which can be estimated as,

$$v_{\text{rot}} = \frac{W_{20}}{2 \sin i}, \quad (7)$$

where i is the inclination angle. W_{20} employed in equation (7) has been corrected for instrumental broadening and redshift (Guo et al. 2020; Catinella et al. 2012; Kent et al. 2008). The errors of W_{20} are estimated following the method described by Guo et al. (2020). Please refer to the *Method* section of their paper for details. In equation (7), we assume an alignment between the inclination angles of the stellar

disk and HI disk in a galaxy and then use the inclination angle of the stellar disk to estimate the rotation velocity. The inclination is estimated from the g -band apparent axis ratio, as (e.g., Guo et al. 2020; Hu et al. 2023; Du et al. 2019; Rong et al. 2024; Begum et al. 2008), $\sin i = \sqrt{\frac{1-(b/a)^2}{1-q_0^2}}$, where q_0 denotes the intrinsic axis ratio seen edge-on. We take $q_0 = 0.2$, which is commonly used in the previous studies (e.g., Du et al. 2019; Guo et al. 2020; Giovanelli et al. 1997; Tully et al. 2009). For those edge-on galaxies with $b/a \leq q_0$, we set $\sin i = 1$.

Previous studies have revealed that the stellar disk and gas disk in galaxies may not be perfectly co-planar, but often exhibit a small inclination difference of $\delta i < 20^\circ$ (e.g., Starkenburg et al. 2019; Guo et al. 2020; Gault et al. 2021). In order to take this misalignment into account, we assume δi following a Gaussian distribution centred at 0° with a standard deviation of $\sigma_i = 20^\circ$. We treat $\sigma_i = 20^\circ$ as the uncertainty associated with i in our study. Note that we do not apply corrections for the velocity dispersion in equation (7), since the effects of the dispersion are severe under $v_{\text{rot}} \lesssim 40$ km/s (summarized by Lelli 2022) while v_{rot} of our sample galaxies are well above ~ 50 km/s.

4 BTFR

In Fig. 3, we observe that the distributions of LSBGs and HSBGs exhibit no significant deviation in the $v_{\text{rot}} - M_b$ diagram. We impose a power-law equation,

$$\log(M_b) = \alpha + \beta \log(v_{\text{rot}}), \quad (8)$$

where α and β are free parameters to fit the BTFRs of the HSBGs and LSBGs using *scipy.odr* package, respectively. To estimate the errors of α and β , we apply the Monte Carlo method. We generate data samples based on the original (v_{rot}, M_b) values and their associated uncertainties. We assume Gaussian distributions for v_{rot} and M_b centered at their origins, with the 1σ regions matching the error bars. This process yields a set of (α, β) values. We repeat this sampling procedure 5,000 times to obtain 5,000 sets of (α, β) values. The standard deviations of these parameters ($\sigma_{x,\text{MC}}$) are then combined with the fitting errors ($\sigma_{x,\text{odr}}$) to determine the uncertainties of α and β , as

$$\sigma_x = \sqrt{\sigma_{x,\text{MC}}^2 + \sigma_{x,\text{odr}}^2}, \quad (9)$$

where the subscript x denotes α or β .

The best-fitting parameters of the BTFR are $\alpha_{\text{HSBG}} = 1.83 \pm 0.51$

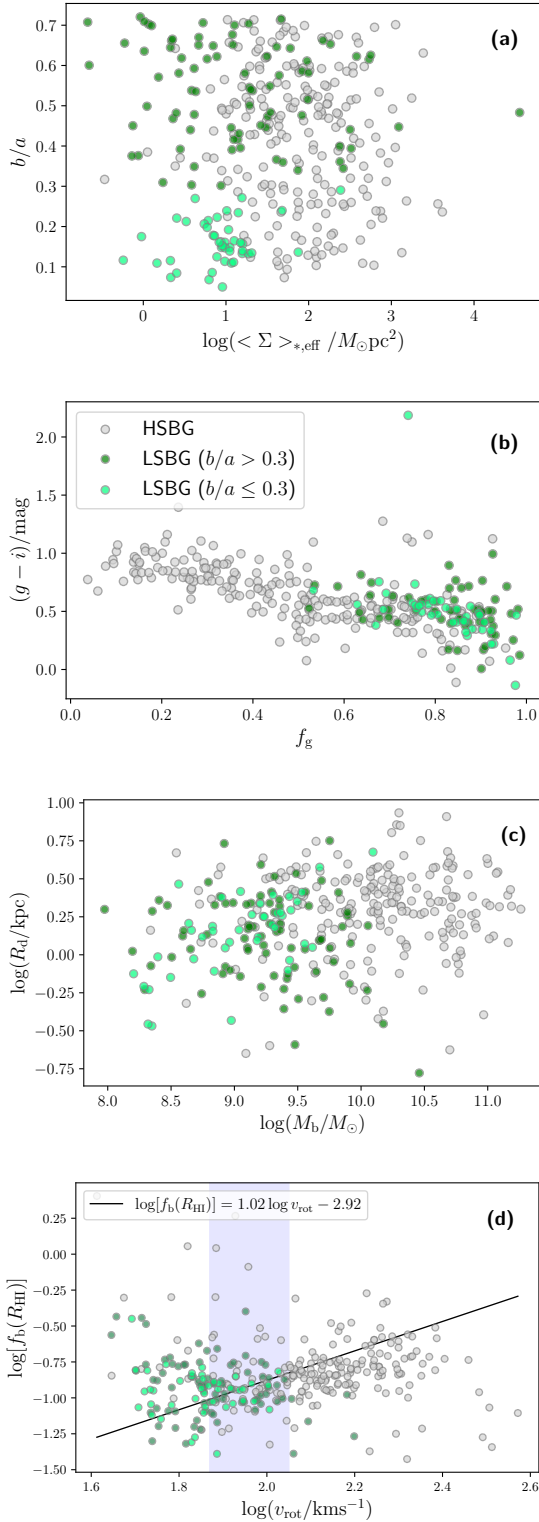


Figure 2. A comparison of properties of selected LSBGs and HSBGs. The green-filled circles represent LSBGs (the dark-green and light-green depict the galaxies with apparent axis ratios $b/a > 0.3$ and $b/a \leq 0.3$, respectively), while the grey-filled circles represent HSBGs. Panel (a): axis ratio b/a versus mean surface density $\langle \Sigma \rangle_{*,\text{eff}}$. Panel (b): $g-i$ color versus gas fraction f_g . Panel (c): scale length R_d versus baryonic mass M_b . Panel (d): v_{rot} versus $f_b(R_{\text{HI}})$. Please refer to Section 2 and Section 5.2 for the definitions of these parameters. The black-solid line and the blue-shaded region in panel d represent the best-fitting linear line and the bin used for performing the two-sample Kuiper tests, respectively, as described in Section 5.2.

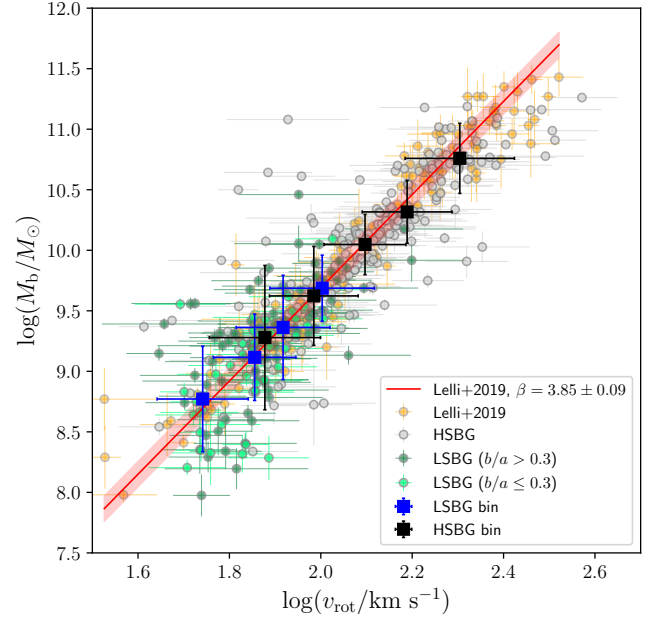


Figure 3. The $v_{\text{rot}} - M_b$ diagram for our samples. The green- and the grey-filled circles are the same as those in Figure 2. The orange-filled circles are SPARC galaxies from Lelli et al. (2019). All the error bars denote 1σ uncertainties. The blue squares represent the median values of LSBGs while the black squares represent those of HSBGs. The red-solid line is the tightest BTFR reported by Lelli et al. (2019). The red-shaded area is the 1σ intrinsic scatter of the red-solid line, which is considered as the 1σ uncertainty of the tightest BTFR.

and $\beta_{\text{HSBG}} = 3.91 \pm 0.24$ for HSBGs, while are $\alpha_{\text{LSBG}} = -1.45 \pm 1.49$ and $\beta_{\text{LSBG}} = 5.67 \pm 0.78$ for LSBGs.

We further split LSBGs and HSBGs into the different $\log v_{\text{rot}}$ bins. Within each bin, we calculate the median value of $\log M_b$ and the corresponding 1σ standard deviation for both samples. As shown in Fig. 3, the binned points of LSBGs (depicted by the blue squares) and HSBGs (depicted as the black squares) comfortably lie within the 1σ uncertainty region of the tightest BTFR of typical late-type galaxies reported by Lelli et al. (2019) (the red-solid line and the red-shaded region denote the best-fitting BTFR of typical late-type galaxies and its 1σ uncertainty, respectively, as shown in Fig. 3), with $\beta \approx 3.85 \pm 0.09$.

Therefore, we conclude that the BTFRs of LSBGs and HSBGs show no significant deviation. Both galaxy samples follow the BTFR of typical late-type galaxies, with a BTFR slope of approximately 4.

Our results are consistent with many previous observational (e.g., McGaugh 2012; Lelli et al. 2016a; Papastergis et al. 2016) and simulation (e.g., Dutton et al. 2017) results. However, it is also noting that some other studies alternatively report smaller slopes ($\beta \sim 3$, e.g., Goddy et al. 2023; Ponomareva et al. 2018).

5 DISCUSSION

5.1 Potential biases

In our study, the SNR threshold used to select the LSBG and HSBG samples may exclude some galaxies with similar HI masses but wider HI line widths, potentially introducing deviations in the slope of the BTFR. To investigate the possible selection effects, we adjust the

SNR threshold by increasing it from 10 to 15, and then to 20. We find that, for HSBGs, the best-fitting β of their BTFR changes to 4.05 ± 0.21 for $\text{SNR} > 15$, and 4.05 ± 0.26 for $\text{SNR} > 20$, still in good agreement with the best-fitting β value for $\text{SNR} > 10$. For LSBGs, the best-fitting β becomes $\sim 6.04 \pm 0.66$ ($\text{SNR} > 15$) and $\sim 6.13 \pm 0.82$ ($\text{SNR} > 20$), which is also similar to the $\beta \sim 5.67 \pm 0.78$ when applying the selection criterion of $\text{SNR} > 10$, considering the large uncertainties of the β values. Additionally, the binned points of LSBGs and HSBGs within different $\log v_{\text{rot}}$ bins for the different SNR thresholds are always located within the 1σ uncertainty region of the BTFR of typical late-type galaxies. Consequently, we conclude that, for both the LSBG and HSBG samples, the selection effect introduced by the SNR threshold is negligible. It should also be noted that, due to the sensitivity limitations of the Arecibo telescope, galaxies with higher rotational velocities v_{rot} exhibit lower signal-to-noise ratios in their HI spectra under a fixed total HI flux, leading to a bias in our parent sample (Haynes et al. 2011; Dou et al. 2024).

Another potential bias may arise from the k_4 cut. Some rotation-supported galaxies with small v_{rot} may exhibit single-horned spectra due to beam-smearing effects (Swaters et al. 2003; Di Teodoro & Fraternali 2015), leading to their exclusion by the k_4 cut. Additionally, galaxies with larger inclination angles tend to have smaller k_4 values (El-Badry et al. 2018). We study the effect of the k_4 cut by adjusting the k_4 threshold from -1.0 to -1.2, and then from -1.0 to -0.8. The BTFR slope of LSBGs changes from $\sim 5.67 \pm 0.78$ ($k_4 < -1.0$) to $\sim 5.38 \pm 0.70$ ($k_4 < -1.2$) and $\sim 4.28 \pm 0.32$ ($k_4 < -0.8$), while the slope of HSBGs changes from $\sim 3.91 \pm 0.24$ ($k_4 < -1.0$) to $\sim 3.78 \pm 0.24$ ($k_4 < -1.2$) and $\sim 3.85 \pm 0.16$ ($k_4 < -0.8$), respectively. It is worth noting that when the k_4 threshold exceeds -0.8, some galaxies appear to deviate from the BTFR. However, these galaxies may be strongly dominated by velocity dispersions, as they typically have unreliable $v_{\text{rot}} \lesssim 40$ km/s (Lelli 2022; El-Badry et al. 2018). Since we cannot determine whether the single-horned HI spectra of these galaxies are due to the beam-smearing effect or the dominance of the velocity dispersions, we keep $k_4 < -1$ to exclude these galaxies.

Additionally, possible bias emerges from using W_{20} or W_{50} (the 50% peak width of an HI spectrum) to estimate the rotation velocities. However, we find that the average difference between the $\log v_{\text{rot}}$ estimated from W_{20} and W_{50} is quite small, even smaller than the uncertainties of $\log v_{\text{rot}}$. Therefore, using W_{20} or W_{50} would not significantly affect our results. Besides, we also test whether using the different methods of estimating M_* (Taylor et al. 2011) or considering the intrinsic thickness q_0 dependence on M_* (Lelli et al. 2016b) would lead to the changes of BTFR slopes of LSBGs. We observe no strong changes in BTFR slopes in these tests. Furthermore, we notice that the surface brightness limit determined by the optical survey may lead to large uncertainties in b/a estimation for LSBGs (Mancera Piña et al. 2024). However, the large uncertainties should result in a larger scatter, rather than a systematic bias or a change of BTFR slope.

5.2 Implications on the formation mechanisms of LSBGs

Previous theoretical studies posit that LSBGs may form in low-density dark matter halos (e.g., Dekel & Silk 1986; McGaugh 1992). However, this model predicts a significant difference in the BTFRs between LSBGs and HSBGs (McGaugh 2021), which contradicts our findings. Therefore, the formation model based on low-density dark matter halos may not refer to LSBGs.

Many observational studies also suggest that LSBGs might be dominated by dark matter compared with HSBGs (e.g., de Blok

& McGaugh 1997; Swaters et al. 2003; Mancera Piña et al. 2022; Read et al. 2017). Therefore, we delve deeper into understanding the fraction of dark matter in LSBGs. Note that BTFR could be expressed as ²,

$$M_b \simeq \frac{f_b^2(R)}{G g_{\text{bar}}(R)} v_{\text{rot}}^4. \quad (10)$$

Here, the baryonic mass fraction within a radius R is defined as $f_b(R) = M_b/M_{\text{tot}}(R)$, where $M_{\text{tot}}(R)$ denotes the total mass enclosed within R . $g_{\text{bar}}(R)$ is the baryonic acceleration at R . $g_{\text{bar}}(R)$ is calculated by assuming the stellar and gas components in a galaxy follow the razor-thin disk distribution, using the method outlined in Read et al. (2017) (see equation (5) of Read et al. (2017) for details).

Note that equation (10) holds true only when R is large. Here, we utilize the HI radius, R_{HI} , defined as the radius where the HI surface density equals $1 M_{\odot}/\text{pc}^2$. R_{HI} can be estimated based on the strong correlation between R_{HI} and M_{HI} (Wang et al. 2016; Gault et al. 2021; Lutz et al. 2018),

$$\log\left(\frac{2R_{\text{HI}}}{\text{kpc}}\right) = (0.506 \pm 0.003) \log\left(\frac{M_{\text{HI}}}{M_{\odot}}\right) - (3.293 \pm 0.009). \quad (11)$$

Consequently, we calculate $f_b(R_{\text{HI}})$ from equation (10) and then analyze the $f_b(R_{\text{HI}}) - v_{\text{rot}}$ relationship for the LSBGs and HSBGs.

As shown in panel (d) of Figure 2, in statistics, $f_b(R_{\text{HI}})$ increases with rising v_{rot} , with a slope of ~ 1.02 using a bisector fitting (Isobe et al. 1990). Since the dark matter halo mass (M_h) of a galaxy is tightly related to v_{rot} , as $M_h \propto v_{\text{rot}}^3$ (Mo et al. 1998), the correlation between $f_b(R_{\text{HI}})$ and v_{rot} hints at a positive association between the baryonic mass fractions and dark matter halo masses for these galaxies (Ayromlou et al. 2023; Duffy et al. 2010). Similar trends have also been observed based on spatially resolved data (e.g., Lelli et al. 2017; Posti et al. 2019; Mancera Piña et al. 2022; Di Teodoro et al. 2023). This correlation does not exceed our expectations, given that our galaxy samples are dominated by the low-mass galaxies. Halos with lower M_h have shallower potentials (Duffy et al. 2010), making it more difficult to prevent the galactic interstellar medium (ISM) against expulsion by the feedback processes in these shallower potentials, which leads to lower $f_b(R_{\text{HI}})$ (e.g., Bryan et al. 2013; Duffy et al. 2010).

Subsequently, in order to compare the $f_b(R_{\text{HI}})$ of the LSBG and HSBG samples with similar dark matter halo masses, we further focus on a specific v_{rot} bin defined by $\log v_{\text{rot}} \in [1.87, 2.05]$ (as depicted by the blue-shaded region in panel (d) of Fig. 2). We have 52 LSBGs and 52 HSBGs in this small bin, exhibiting similar distributions of v_{rot} with median $\log v_{\text{rot}}$ values of 1.94 ± 0.05 (for LSBGs) and 1.97 ± 0.05 (for HSBGs). The Kuiper test between the distributions of v_{rot} of LSBGs and HSBGs in this small bin also gives a large p -value of 0.77, indicating no significant difference in v_{rot} . We then compare the $f_b(R_{\text{HI}})$ distributions of the LSBG and HSBG sample galaxies within this v_{rot} bin. The median values of the $f_b(R_{\text{HI}})$ distributions of LSBGs and HSBGs are -0.94 ± 0.15 and -0.91 ± 0.30 , respectively; the Kuiper test for the two $f_b(R_{\text{HI}})$ distributions also yields a large p -value of 0.34.

Therefore, we note that, for LSBGs and HSBGs with similar halo masses, their baryonic fractions are also comparable. LSBGs may not be particularly dark matter-dominated galaxies compared to their HSBG counterparts; at least within the regimes of R_{HI} , the dark matter fractions of LSBGs and HSBGs are similar. Furthermore, this

² Equation (10) is from the lecture on the Tully-Fisher relation; see also Aaronson et al. (1979) and Zwaan et al. (1995).

result also plausibly suggests comparable feedback power among the LSBGs and HSBGs with similar halo masses (i.e., similar gravitational potentials). Consequently, we conclude that feedback may not be the primary driver of the different surface brightness between these HI-bearing galaxies. In other words, these HI-bearing LSBGs may not originate from stronger or weaker feedback.

Alternatively, our finding aligns with the simulation results where the LSBGs can be well reproduced by higher dark matter halo spins (e.g., Pérez-Montaño et al. 2022; Di Cintio et al. 2019). Therefore, we conclude that our result may lend support to the theorem that LSBGs may originate from high-spin dark matter halos (e.g., Mo et al. 1998).

Except for the aforementioned formation models of LSBGs in the framework of Λ CDM, MOND may also offer a reasonable explanation for the BTFR of LSBGs (e.g., Milgrom 1983; Wittenburg et al. 2020). As demonstrated in Section 4, both LSBGs and HSBGs follow a BTFR with a slope indistinguishable from 4. This result adheres to the theoretical predictions by MOND (Milgrom 1983). Therefore, our result cannot exclude the MOND theory. Nevertheless, several studies on the dynamics of galaxies have produced results that deviate from MOND's predictions (e.g., Ren et al. 2019; Mercado et al. 2024; Mancera Piña et al. 2024; Khelashvili et al. 2024). Therefore, more compelling studies are needed to better determine if MOND is a promising framework.

6 SUMMARY

Taking advantage of the ALFALFA HI survey data, we have selected the HI-bearing LSBGs and HSBGs, and estimated their baryonic masses M_b and rotation velocities v_{rot} . Our findings reveal that, statistically, the HI-bearing LSBGs and HSBGs also conform to the BTFR found in typical late-type galaxies as well as ordinary dwarf galaxies with slope ~ 4 . These results hint that LSBGs may owe their properties to the high spins of their host dark matter halos, rather than the halo densities or feedback processes. Additionally, our findings do not rule out the Modified Newtonian Dynamics (MOND) theory.

Our findings conflict with the BTFR results of UDGs (Mancera Piña et al. 2019; Guo et al. 2020; Hu et al. 2023; Karunakaran et al. 2020; Rong et al. 2024). This is primarily because that our LSBG sample contains very few UDGs. Indeed, almost all of our LSBGs are classic LSBGs, rather than UDGs with extremely large effective radii. Therefore, we propose that UDGs may be a distinct galaxy population with different BTFR and mass distributions, compared with classical LSBGs. They may also have distinct formation mechanisms that warrant further investigations.

ACKNOWLEDGEMENTS

We express our sincere thanks to the referee for the detailed comments and suggestions. We also thank Xufen Wu, Haochen Jiang, Jingshuo Yang, Shijiang Chen and Yu Chen for the inspiring discussions during this study. Y.R. acknowledges supports from the NSFC grant 12273037, the CAS Pioneer Hundred Talents Program (Category B), the USTC Research Funds of the Double First-Class Initiative (No. YD2030002013), and the research grants from the China Manned Space Project (the second-stage CSST science projects: "Investigation of small-scale structures in galaxies and forecasting of observations" and "CSST study on specialized galaxies in ultraviolet and multi-band"). H.H. is supported by the Fundamental Research

Funds for the Central Universities, the CAS Project for Young Scientists in Basic Research Grant No. YSBR-062, the National SKA Program of China No. 2022SKA0110201, and the NSFC grant No. 12033008.

DATA AVAILABILITY

Data are available if requested.

REFERENCES

- Aarson M., Huchra J., Mould J., 1979, *ApJ*, **229**, 1
 Amorisco N. C., Loeb A., 2016, *MNRAS*, **459**, L51
 Ayromlou M., Nelson D., Pillepich A., 2023, *MNRAS*, **524**, 5391
 Begum A., Chengalur J. N., Karachentsev I. D., Sharina M. E., 2008, *MNRAS*, **386**, 138
 Bothun G., Impey C., McGaugh S., 1997, *PASP*, **109**, 745
 Bryan S. E., Kay S. T., Duffy A. R., Schaye J., Dalla Vecchia C., Booth C. M., 2013, *MNRAS*, **429**, 3316
 Carleton T., Errani R., Cooper M., Kaplinghat M., Peñarrubia J., Guo Y., 2019, *MNRAS*, **485**, 382
 Catinella B., et al., 2012, *MNRAS*, **420**, 1959
 Catinella B., et al., 2018, *MNRAS*, **476**, 875
 Chan T. K., Kereš D., Wetzel A., Hopkins P. F., Faucher-Giguère C. A., El-Badry K., Garrison-Kimmel S., Boylan-Kolchin M., 2018, *MNRAS*, **478**, 906
 Dekel A., Silk J., 1986, *ApJ*, **303**, 39
 Di Cintio A., Brook C. B., Macciò A. V., Dutton A. A., Cardona-Barrero S., 2019, *MNRAS*, **486**, 2535
 Di Teodoro E. M., Fraternali F., 2015, *MNRAS*, **451**, 3021
 Di Teodoro E. M., et al., 2023, *MNRAS*, **518**, 6340
 Dou J., et al., 2024, *ApJ*, **973**, L23
 Du W., Wu H., Lam M. I., Zhu Y., Lei F., Zhou Z., 2015, *AJ*, **149**, 199
 Du W., Cheng C., Wu H., Zhu M., Wang Y., 2019, *MNRAS*, **483**, 1754
 Duffy A. R., Schaye J., Kay S. T., Dalla Vecchia C., Battye R. A., Booth C. M., 2010, *MNRAS*, **405**, 2161
 Dutton A. A., 2012, *MNRAS*, **424**, 3123
 Dutton A. A., et al., 2017, *MNRAS*, **467**, 4937
 El-Badry K., et al., 2018, *MNRAS*, **477**, 1536
 Galaz G., Dalcanton J. J., Infante L., Treister E., 2002, *AJ*, **124**, 1360
 Galaz G., Herrera-Camus R., Garcia-Lambas D., Padilla N., 2011, *ApJ*, **728**, 74
 Gault L., et al., 2021, *ApJ*, **909**, 19
 Giovanelli R., Haynes M. P., Herter T., Vogt N. P., Wegner G., Salzer J. J., da Costa L. N., Freudling W., 1997, *AJ*, **113**, 22
 Goddy J. S., Stark D. V., Masters K. L., Bundy K., Drory N., Law D. R., 2023, *MNRAS*, **520**, 3895
 Governato F., et al., 2010, *Nature*, **463**, 203
 Guo Q., et al., 2020, *Nature Astronomy*, **4**, 246
 Haynes M. P., et al., 2011, *AJ*, **142**, 170
 Haynes M. P., et al., 2018, *ApJ*, **861**, 49
 He M., Wu H., Du W., Liu H.-y., Lei F.-j., Zhao P.-s., Zhang B.-q., 2020, *ApJS*, **248**, 33
 Hu H.-J., Guo Q., Zheng Z., Yang H., Tsai C.-W., Zhang H.-X., Zhang Z.-Y., 2023, *ApJ*, **947**, L9
 Impey C., Bothun G., 1997, *ARA&A*, **35**, 267
 Isobe T., Feigelson E. D., Akritas M. G., Babu G. J., 1990, *ApJ*, **364**, 104
 Karunakaran A., Spekkens K., Zaritsky D., Donnerstein R. L., Kadowaki J., Dey A., 2020, *ApJ*, **902**, 39
 Kent B. R., et al., 2008, *AJ*, **136**, 713
 Khelashvili M., Rudakovskiy A., Hossenfelder S., 2024, *arXiv e-prints*, p. arXiv:2401.10202
 Kim J.-h., Lee J., 2013, *MNRAS*, **432**, 1701
 Kulier A., Galaz G., Padilla N. D., Trayford J. W., 2020, *MNRAS*, **496**, 3996

- Kuzio de Naray R., McGaugh S. S., de Blok W. J. G., 2004, *MNRAS*, **355**, 887
- Lelli F., 2022, *Nature Astronomy*, **6**, 35
- Lelli F., Fraternali F., Sancisi R., 2010, *A&A*, **516**, A11
- Lelli F., McGaugh S. S., Schombert J. M., 2016a, *ApJ*, **816**, L14
- Lelli F., McGaugh S. S., Schombert J. M., Pawlowski M. S., 2016b, *ApJ*, **827**, L19
- Lelli F., McGaugh S. S., Schombert J. M., Pawlowski M. S., 2017, *ApJ*, **836**, 152
- Lelli F., McGaugh S. S., Schombert J. M., Desmond H., Katz H., 2019, *MNRAS*, **484**, 3267
- Lutz K. A., et al., 2018, *MNRAS*, **476**, 3744
- Mancera Piña P. E., Peletier R. F., Aguerri J. A. L., Venhola A., Trager S., Choque Challapa N., 2018, *MNRAS*, **481**, 4381
- Mancera Piña P. E., et al., 2019, *ApJ*, **883**, L33
- Mancera Piña P. E., et al., 2020, *MNRAS*, **495**, 3636
- Mancera Piña P. E., Fraternali F., Oosterloo T., Adams E. A. K., di Teodoro E., Bacchini C., Iorio G., 2022, *MNRAS*, **514**, 3329
- Mancera Piña P. E., Golini G., Trujillo I., Montes M., 2024, *arXiv e-prints*, p. [arXiv:2404.06537](https://arxiv.org/abs/2404.06537)
- Martin G., et al., 2019, *MNRAS*, **485**, 796
- McGaugh S. S., 1992, PhD thesis, University of Michigan
- McGaugh S. S., 2012, *AJ*, **143**, 40
- McGaugh S. S., 2021, *Studies in History and Philosophy of Science*, **88**, 220
- McGaugh S. S., Schombert J. M., 2015, *ApJ*, **802**, 18
- McGaugh S. S., Schombert J. M., Bothun G. D., de Blok W. J. G., 2000, *ApJ*, **533**, L99
- McGaugh S. S., Lelli F., Schombert J. M., 2016, *Phys. Rev. Lett.*, **117**, 201101
- Mercado F. J., Bullock J. S., Moreno J., Boylan-Kolchin M., Hopkins P. F., Wetzel A., Faucher-Giguère C.-A., Samuel J., 2024, *MNRAS*, **530**, 1349
- Milgrom M., 1983, *ApJ*, **270**, 371
- Mo H. J., McGaugh S. S., Bothun G. D., 1994, *MNRAS*, **267**, 129
- Mo H. J., Mao S., White S. D. M., 1998, *MNRAS*, **295**, 319
- Mowla L., van Dokkum P., Merritt A., Abraham R., Yagi M., Koda J., 2017, *ApJ*, **851**, 27
- Noguchi M., 2001, *MNRAS*, **328**, 353
- Papastergis E., Adams E. A. K., van der Hulst J. M., 2016, *A&A*, **593**, A39
- Papastergis E., Adams E., Romanowsky A., 2017, *Astronomy & Astrophysics*, **601**, L10
- Pérez-Montaño L. E., Cervantes Sodi B., 2019, *MNRAS*, **490**, 3772
- Pérez-Montaño L. E., Rodríguez-Gomez V., Cervantes Sodi B., Zhu Q., Pillepich A., Vogelsberger M., Hernquist L., 2022, *MNRAS*, **514**, 5840
- Piontek F., Steinmetz M., 2011, *MNRAS*, **410**, 2625
- Ponomareva A. A., Verheijen M. A. W., Papastergis E., Bosma A., Peletier R. F., 2018, *MNRAS*, **474**, 4366
- Posti L., Marasco A., Fraternali F., Famaey B., 2019, *A&A*, **629**, A59
- Prole D. J., et al., 2019, *MNRAS*, **484**, 4865
- Read J. I., Iorio G., Agertz O., Fraternali F., 2017, *MNRAS*, **467**, 2019
- Ren T., Kwa A., Kaplinghat M., Yu H.-B., 2019, *Physical Review X*, **9**, 031020
- Rong Y., Guo Q., Gao L., Liao S., Xie L., Puzia T. H., Sun S., Pan J., 2017, *MNRAS*, **470**, 4231
- Rong Y., Dong X.-Y., Puzia T. H., et al. 2020a, *ApJ*, **899**, 78
- Rong Y., Zhu K., Johnston E. J., Zhang H.-X., Cao T., Puzia T. H., Galaz G., 2020b, *ApJ*, **899**, L12
- Rong Y., Hu H., He M., Du W., Guo Q., Wang H.-Y., Zhang H.-X., Mo H., 2024, *arXiv e-prints*, p. [arXiv:2404.00555](https://arxiv.org/abs/2404.00555)
- Saburova A. S., Chilingarian I. V., Katkov I. Y., Egorov O. V., Kasparova A. V., Khoperskov S. A., Uklein R. I., Vozyakova O. V., 2018, *MNRAS*, **481**, 3534
- Saburova A. S., Chilingarian I. V., Kasparova A. V., Katkov I. Y., Fabricant D. G., Uklein R. I., 2019, *MNRAS*, **489**, 4669
- Saburova A. S., Chilingarian I. V., Kasparova A. V., Sil'chenko O. K., Grishin K. A., Katkov I. Y., Uklein R. I., 2021, *MNRAS*, **503**, 830
- Sales L. V., et al., 2017, *MNRAS*, **464**, 2419
- Schombert J., McGaugh S., 2021, *AJ*, **161**, 91
- Serra P., et al., 2012, *MNRAS*, **422**, 1835
- Smith J. A., et al., 2002, *AJ*, **123**, 2121
- Starkenburger T. K., Sales L. V., Genel S., Manzano-King C., Canalizo G., Hernquist L., 2019, *ApJ*, **878**, 143
- Swaters R. A., Madore B. F., van den Bosch F. C., Balcells M., 2003, *ApJ*, **583**, 732
- Taylor E. N., et al., 2011, *MNRAS*, **418**, 1587
- Tully R. B., Rizzi L., Shaya E. J., Courtois H. M., Makarov D. I., Jacobs B. A., 2009, *AJ*, **138**, 323
- Verheijen M. A. W., 1997, PhD thesis, Univ. Groningen
- Verheijen M. A. W., 2001, *ApJ*, **563**, 694
- Wang J., Koribalski B. S., Serra P., van der Hulst T., Roychowdhury S., Kamphuis P., Chengalur J. N., 2016, *MNRAS*, **460**, 2143
- Wittenburg N., Kroupa P., Famaey B., 2020, *ApJ*, **890**, 173
- Wright E. L., et al., 2010, *AJ*, **140**, 1868
- Wright A. C., Tremmel M., Brooks A. M., Munshi F., Nagai D., Sharma R. S., Quinn T. R., 2021, *MNRAS*, **502**, 5370
- Wyder T. K., et al., 2009, *ApJ*, **696**, 1834
- Zhong W., Fu J., Sharma P., Shen S., Yates R. M., 2023, *MNRAS*, **519**, 4344
- Zhu Q., Pérez-Montaño L. E., Rodríguez-Gomez V., Cervantes Sodi B., Zjupa J., Marinacci F., Vogelsberger M., Hernquist L., 2023, *MNRAS*, **523**, 3991
- Zwaan M. A., van der Hulst J. M., de Blok W. J. G., McGaugh S. S., 1995, *MNRAS*, **273**, L35
- de Blok W. J. G., McGaugh S. S., 1997, *MNRAS*, **290**, 533
- den Heijer M., et al., 2015, *A&A*, **581**, A98
- van Dokkum P. G., Abraham R., Merritt A., Zhang J., Geha M., Conroy C., 2015a, *ApJ*, **798**, L45
- van Dokkum P. G., et al., 2015b, *ApJ*, **804**, L26
- van Dokkum P., et al., 2018, *Nature*, **555**, 629

This paper has been typeset from a $\text{\TeX}/\text{\LaTeX}$ file prepared by the author.